



# Sulfur mass-independent fractionation in liquid phase chemistry: UV photolysis of phenacylphenylsulfone as a case study

Sebastian Kopf<sup>1</sup>, Shuhei Ono<sup>\*</sup>

*Department of Earth, Atmospheric, and Planetary Sciences, Massachusetts Institute of Technology, 77 Massachusetts Avenue, Cambridge, MA 02139, United States*

Received 8 March 2011; accepted in revised form 7 February 2012; available online 3 March 2012

## Abstract

The sulfur isotope mass-independent fractionation (S-MIF) represents a distinct geochemical signature commonly observed in Archean rocks. Although S-MIF is generally thought to be exclusive to gas phase chemistry, several studies have suggested that liquid phase or heterogeneous chemistry may also produce S-MIF signatures.

This study investigates the potential contribution of the poorly explored mass-independent effects from liquid phase sulfur chemistry. Our investigation focused on laboratory experiments of the UV photolysis of phenacylphenylsulfone as a model system. This system was chosen due to previous measurements of  $\Delta^{33}\text{S}$  (not  $\Delta^{36}\text{S}$ ) by a low precision  $\text{SO}_2$  method indicating the occurrence of anomalous fractionation in  $^{33}\text{S}$ .

The photolysis of PPS in micellar solution produced MIF of  $^{33}\text{S}$  in residual PPS ranging from depletion by  $-2.1\text{‰}$  to enrichment by  $6.4\text{‰}$ , with small mass-dependent fractionation of  $\delta^{34}\text{S}$  up to  $2.1\text{‰}$ . While this magnitude of  $^{33}\text{S}$  anomaly is comparable to the range of values observed in Archean rocks, no anomaly in  $^{36}\text{S}$  was detected for the  $^{32}\text{S}$ – $^{34}\text{S}$ – $^{36}\text{S}$  system beyond analytical precision ( $0.19\text{‰}$ ). These results confirm the anomalous fractionation to be caused most likely by magnetic isotope effects (MIE), affecting only the nuclear spin possessing  $^{33}\text{S}$  among the four stable isotopes of sulfur. The observed initial depletion of  $^{33}\text{S}$  in the reactant PPS was unexpected and suggests changing contributions of at least two spin-selective processes. The results of this study demonstrate that liquid phase processes, such as the photolysis of certain organic sulfur compounds, can produce anomalous  $^{33}\text{S}$  abundance.

© 2012 Elsevier Ltd. All rights reserved.

## 1. INTRODUCTION

Sedimentary sulfide and sulfate minerals from Archean and Early Proterozoic rocks older than 2.4 billion years commonly exhibit sulfur isotope signatures that are mass-

independently fractionated<sup>2</sup> (e.g., Farquhar et al., 2000a; Pavlov and Kasting, 2002; Ono et al., 2003; Kaufman et al., 2007). Traditional geochemical processes (e.g., biological and hydrothermal reactions) and sulfur cycling

<sup>2</sup> Equilibrium, kinetic and biological processes nominally fractionate the four stable isotopes of sulfur ( $^{32}\text{S}$ ,  $^{33}\text{S}$ ,  $^{34}\text{S}$  and  $^{36}\text{S}$ ) in proportion to their differences in mass as predicted by the quantum mechanical theory of isotope fractionation (Bigeleisen and Mayer, 1947; Urey, 1947; Young et al., 2002). As a result, they produce mass-dependent isotope fractionation (MDF), where fractionation scales to the mass difference. Mass-independent fractionation (or non-mass dependent fractionation) of sulfur refers to isotopic compositions that deviate strongly from this mass scaling law.

\* Corresponding author.

*E-mail address:* [sono@mit.edu](mailto:sono@mit.edu) (S. Ono).

<sup>1</sup> Present address: Division of Geological and Planetary Sciences, California Institute of Technology, 1200 East California Boulevard, Pasadena, CA 91125, United States.

cannot readily explain these large deviations from mass-dependent behavior. The origin of the MIF effects was hypothesized to be atmospheric (Farquhar et al., 2000a) and modeling studies on the constraints for preserving such an atmospheric MIF signal in the rock record have since provided evidence for a mostly anoxic Archean atmosphere and rise of atmospheric oxygen above a few ppm levels only after 2.3 Ga (Pavlov and Kasting, 2002). By today, the disappearance of sulfur MIF from the rock record is widely recognized as one of the most reliable proxies for the rise of atmospheric oxygen in the Early Proterozoic (Farquhar et al., 2000a; Farquhar et al., 2001; Kasting, 2001; Pavlov and Kasting, 2002; Farquhar and Wing, 2003; Mojzsis et al., 2003; Ono et al., 2003; Bekker et al., 2004; Farquhar et al., 2007), however, the processes and exact mechanisms of mass-independent sulfur fractionation in the Archean remain poorly understood.

Mass-independent effects in gas phase chemistry were observed for oxygen ( $^{16}\text{O}$ – $^{17}\text{O}$ – $^{18}\text{O}$ ) as early as 1983 (Thiemens and Heidenreich, 1983; Gao and Marcus, 2002; Thiemens, 2006) and were suspected to exist for the sulfur isotope system as well. A number of gas phase processes for potentially relevant sulfur gases have since been investigated both theoretically and experimentally, such as photolysis of  $\text{SO}_2$  (Farquhar et al., 2001; Danielache et al., 2008b; Masterson et al., 2011),  $\text{H}_2\text{S}$  (Farquhar et al., 2000b),  $\text{OCS}$  (Danielache et al., 2008a, 2011) and  $\text{SO}_3$  (Pavlov et al., 2005) as well as photopolymerization of  $\text{CS}_2$  (Zmolek et al., 1999), recombination of  $\text{S}_3$  (Francisco et al., 2005) and  $\text{SO}_2$  self-shielding (Lyons, 2008; Lyons, 2009).

While these studies support the model of atmospheric origin of Archean S-MIF, it has been recognized that MIF is not entirely exclusive to gas phase chemistry. Previously investigated non gas phase reactions and mechanisms include magnetic isotope effects (Turro and Kraeutler, 1980; Buchachenko, 2001), nuclear volume effects (Bigeleisen, 1996; Schauble, 2007), surface adsorption (Lasaga et al., 2008), thermochemical sulfate reduction (Watanabe et al., 2009; Oduru et al., 2011) and fluorination of metal sulfides (Cartigny et al., 2008). To this date, particularly little attention has been granted to liquid phase processes, largely due to the lack of known mechanisms for mass-independent fractionation of  $^{36}\text{S}$ . Following magnetic field experiments by Hayashi et al. (1987), a study by Step et al. (1992) investigated aqueous-phase photolysis of phenacylphenylsulfone (PPS) for its sensitivity to magnetic field effects, but in the process also observed it to produce mass-independent  $^{33}\text{S}$  fractionation in two measurements of the  $^{32}\text{S}$ – $^{33}\text{S}$ – $^{34}\text{S}$  system ( $^{36}\text{S}$  was not measured in their study). They hypothesized the effect to be spin-selective in nature, i.e. due to a magnetic isotope effect that fractionates the magnetic  $^{33}\text{S}$  isotope mass-independently, but were surprised to find it unexpectedly weak for a magnetic isotope effect. The system furthermore produced this isotope effect while operating at a wavelength of 280–350 nm without the need for UV-C radiation (100–280 nm), allowing for this process to take place in the presence of weak ozone shielding in an already slightly oxic atmosphere (Farquhar et al., 2001), potentially removing the constraint on atmospheric oxygen imposed by gas phase MIF. Inspired by the experimental results from the

Scheme 1

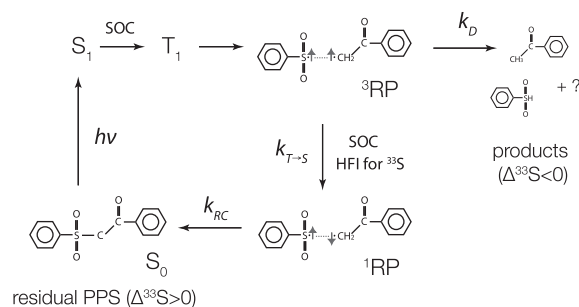


Fig. 1. Original reaction scheme suggested for PPS photolysis. Intersystem crossing (ISC) by hyperfine interaction (HFI) during spin conversion of triplet ( $^3\text{RP}$ ) to singlet radical pair ( $^1\text{RP}$ ) is accelerated by the magnetic isotope  $^{33}\text{S}$  and produces a magnetic isotope effect. Mechanisms, electronic states and pathways mentioned in the text are indicated: spin-orbit coupling (SOC); ground state ( $\text{S}_0$ ), excited singlet ( $\text{S}_1$ ) and triplet ( $\text{T}_1$ ) PPS; radical pair diffusion ( $k_D$ ); triplet-singlet ( $k_{\text{T-S}}$ ) ISC; RP recombination to PPS ( $k_{\text{RC}}$ ).

earlier investigation by Step et al. (1992), this study intends to mend the gap by exploring the quadruple sulfur isotope fractionation during liquid phase UV photolysis of PPS as a model system for initial investigation of liquid phase processes. In particular, high precision measurements of  $^{36}\text{S}$  are carried out to test if the anomalous isotope effect is only observed in the magnetic isotope  $^{33}\text{S}$ .

### 1.1. MIE during PPS photolysis

Scheme 1 (Fig. 1) illustrates the original model of PPS photolysis proposed by Step et al. (1992). PPS photolysis takes place inside the micellar cage of sodium dodecyl sulfate (SDS). Ground state PPS ( $\text{S}_0$ ) absorbs a photon to produce the electronically excited singlet state ( $\text{S}_1$ ), which undergoes rapid intersystem crossing (ISC) through electron spin-orbit coupling (SOC) to generate triplet PPS ( $\text{T}_1$ ) and breaks at the weak carbon–sulfur bond to form a triplet state radical pair ( $^3\text{RP}$ ) consisting of benzoylmethyl and phenylsulphonyl radicals. The radical pair at this point has two escape pathways, (1) it either diffuses, separates completely and reacts with the micellar cage or the aqueous medium outside the micelle ( $k_D$ ) to form acetophenone, sulfonic acids and other non-specific products, or (2) granted its lifetime is long enough to allow the relatively slow ISC mechanisms to occur, it undergoes triplet-singlet ISC through electron–nuclear hyperfine interactions (HFI) to singlet ground state ( $k_{\text{T-S}}$ ) and recombines to PPS ( $k_{\text{RC}}$ ). The hyperfine interaction between the magnetic  $^{33}\text{S}$  nuclei and electron spin moments accelerates the triplet-singlet conversion of radical pairs ( $k_{\text{T-S}}$ ) by either rephasing of the two electron spin angular momenta in the radical pair ( $\text{T}_0 \rightarrow \text{S}$ ), or by coupled flips in the spin directions of electron and magnetic nuclei ( $\text{T}_+$  or  $\text{T}_- \rightarrow \text{S}$ ).<sup>3</sup> This scenario (Fig. 1) produces a magnetic isotope effect by

<sup>3</sup> Triplet state has three non-degenerate energy levels that correspond to angular momentum of a pair of electrons to be either out of phase,  $\text{T}_0$ , or in the same directions,  $\text{T}_+$  or  $\text{T}_-$ .

hyperfine interactions during recombination of the triplet radical pair (Buchachenko, 2001; Turro and Kraeutler, 1980; Turro, 1983).

## 2. MATERIALS AND METHODS

### 2.1. Materials

Phenacylphenylsulfone (PPS, CAS 3406-03-9) was purchased from the rare chemicals library of Sigma–Aldrich (S596736). All other chemicals used in the experiment are off-the-shelf high grade laboratory chemicals from Sigma–Aldrich (HPLC grade for solvents, ACS grade for concentrated acids). High purity (>99.8%) compressed oxygen was purchased from AirGas. Micellar solution of SDS was prepared by dissolving SDS in deionized water above the critical micelle concentration (8.2 mM). PPS stock solution was prepared by dissolving 1 mM PPS in 100 mM SDS solution with continuous stirring at low heat for 10 h. The absorption spectrum of the stock solution was measured against a water blank in a quartz cuvette with 1 cm pathlength at a dilution of 1:10 using a Shimadzu UV-2450 spectrophotometer (Fig. 2).

### 2.2. Photolysis

Aliquots of 120 mL PPS stock solution were photolyzed in a 120 mL quartz flask for 0, 2.5, 7.5, 12.5, 17.5 and 27.5 min of light exposure from the full spectrum of a 150W Xenon lamp (Newport model 6254) as well as with the truncated spectrum from the same lamp using a glass filter to block radiation below 280 nm (similar to the light regime used in the experiments by Step et al. (1992)). PPS absorbs UV light in both wavelength bands (full spectrum and filtered light) with a major absorption peak at 254 nm only accessible during full spectrum photolysis (Fig. 2). The irradiance of the Xenon lamp decreases at lower wavelengths such that expected photon flux at 250 nm is ~45% of photon flux at 300 nm. Light transmission of the quartz flask and the deionized water used to make the

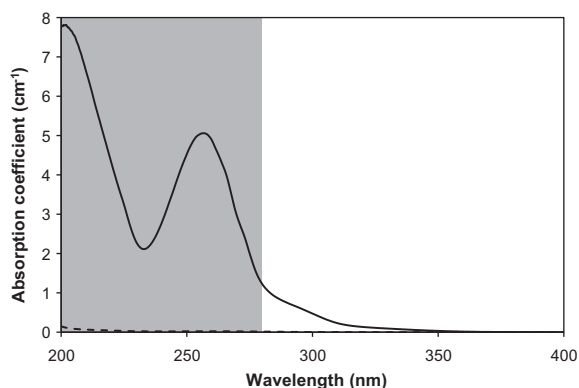


Fig. 2. Absorption spectrum of 0.1 mM PPS in 10 mM SDS solution (1:10 dilution of experimental concentrations) and background absorption of 10 mM SDS (dashed line), measured at 0.1 nm resolution, relative to pure deionized water. Area shaded in gray indicates spectral range filtered out in experiments with >280 nm filtered light regime.

PPS solution is >93% at wavelengths  $\geq 250$  nm (Quickenden and Irvin, 1980). According to the absorption spectrum measured in Fig. 2, we estimate that during the experiment, >99% of the photons at 250, 280 and 300 nm are absorbed by the PPS solution within 0.1, 0.4 and 1.0 cm from the wall of the reaction vessel, respectively.

Concentration of PPS before and after photolysis was measured at  $\lambda = 254$  nm by methanol gradient HPLC with a Symmetry C18 column (5  $\mu\text{m}$  4.6  $\times$  250 mm) and 168 Diode Array Detector, using a four point calibration curve. Acetophenone was the only reaction product detected by HPLC. None of the sulfur-bearing products could be identified by HPLC or by earlier attempts by Step et al. (1992) using gas chromatography. Identification and isotopic analysis of the sulfur-bearing reaction products was not pursued further. The stock solutions used for full spectrum and filtered light experiments contained 1.00 and 1.07 mM PPS, respectively.

### 2.3. Extraction and sulfur isotope analysis

PPS was extracted from the micellar solution twice with 200 mL 4:1 (v/v) ethyl acetate:dichloromethane and purified on a silica column using 3% isopropanol (v%), 15% ethyl acetate (v%) in hexane as the eluent. Purified PPS was crystallized from hexane and combusted with 900 mg starch at 30 atm  $\text{O}_2$  in a Parr 1108 Oxygen Combustion Bomb (Arikawa and Sasaki, 1987) to oxidize the sulfonyl group to sulfate. Five milliliters sodium carbonate solution (50 g/L) was used as absorbent. Reaction products were collected with 300 mL deionized water, acidified to  $\text{pH} < 3$  and spiked with 10 mL bromine water to fully oxidize any residual sulfur intermediates. After evaporation to 50 mL, sulfate was precipitated as barium sulfate by addition of 5 mL 0.4 M barium chloride, washed with deionized water and dried for further processing. Combustion of starch was used as procedural blank and yielded no detectable barium sulfate, indicating combustion to be free of sulfur-bearing contaminants.

A mixture of hydroiodic, hypophosphorous and hydrochloric acid (Thode et al., 1961) was used to reduce the collected barium sulfate to hydrogen sulfide (Forrest and Newman, 1977). Hydrogen sulfide was captured in a zinc acetate trap as zinc sulfide and preserved as silver sulfide by precipitation with 5 mL 0.1 M silver nitrate. Silver sulfide was reacted over-night, washed several times with deionized water and dried for subsequent isotope analysis.

Sulfur isotope ratio analysis of silver sulfide was carried out following the procedure described by Ono et al. (2006b): 2 mg samples of silver sulfide were reacted with fluorine gas in externally heated nickel tubes at 300  $^\circ\text{C}$  to form  $\text{SF}_6$ . After GC purification of  $\text{SF}_6$ , the  $^{32}\text{SF}_5^+$ ,  $^{33}\text{SF}_5^+$ ,  $^{34}\text{SF}_5^+$  and  $^{36}\text{SF}_5^+$  ions were analyzed by a Thermo-Electron MAT 253 isotope ratio mass-spectrometer.

### 2.4. Notation

Sulfur isotope compositions are expressed in the conventional  $\delta$  notation as deviations in isotope ratios of the sample ( $^x\text{R}_{sa}$ ) with respect to the initial reactant PPS ( $^x\text{R}_i$ ):

$$\delta^x\text{S} = \frac{{}^x\text{R}_{sa}}{{}^x\text{R}_i} - 1 \quad (1)$$

where,  ${}^x\text{R}$  is the ratio  ${}^x\text{S}/{}^{32}\text{S}$  with  $x = 33, 34$  or  $36$  (and multiplied by 1000 to be presented as ‰). The following capital delta notation is used as a measure of anomalous  ${}^{33}\text{S}$  and  ${}^{36}\text{S}$  abundance (Angert et al., 2003; Ono et al., 2003):

$$\Delta^{33}\text{S} = \ln(\delta^{33}\text{S} + 1) - 0.515 \times \ln(\delta^{34}\text{S} + 1) \quad (2)$$

$$\Delta^{36}\text{S} = \ln(\delta^{36}\text{S} + 1) - 1.90 \times \ln(\delta^{34}\text{S} + 1) \quad (3)$$

## 2.5. Error estimation

Overall yield of the experimental procedure from initial photolysis to recovery of silver sulfide was consistent across all samples with an average  $47.5 \pm 9.4\%$  recovery. Measurements of PPS concentrations before, and barium sulfate weight after combustion, indicated that most losses occurred at the combustion step, which was tested carefully for isotope fractionation effects with PPS and cysteine (Table 1). Despite non-quantitative recovery through the elaborate procedure, the  $\delta^{34}\text{S}$  value for cysteine and PPS was reproducible within  $1.9\%$  and  $0.3\%$ , respectively. This suggests that there were no major mass-dependent isotope effects during the extraction process. The error from extraction, combustion and reduction procedures in combination with errors from the fluorination analysis itself is estimated at  $1.1\%$  ( $2\sigma$ ) for  $\delta^{34}\text{S}$  from quadruplicate cysteine combustion as well as triplicate PPS controls (Table 1). Errors in  $\Delta^{33}\text{S}$  and  $\Delta^{36}\text{S}$  are estimated at  $0.014$  and  $0.19\%$  ( $2\sigma$ ), respectively, from replicate ( $N = 28$ ) analysis of international reference materials. The error in PPS quantification was estimated at  $0.049$  mM ( $2\sigma$ ) from 10 replicate measurements of the PPS stock solutions.

## 3. RESULTS

Both during full spectrum photolysis, as well as with filtered light, PPS degradation followed first-order kinetics (Eq. (4)) until approximately 45% of the initial PPS was degraded (indicated by transition from solid to dashed regression lines in Fig. 3).

$$\frac{d[\text{PPS}]}{dt} = -k[\text{PPS}] \quad (4)$$

Table 1

Multiple sulfur isotope composition of cysteine and PPS from control experiments. Isotopic values are reported with respect to average PPS.

$\delta^{33}\text{S}$ (‰)	$\delta^{34}\text{S}$ (‰)	$\delta^{36}\text{S}$ (‰)	$\Delta^{33}\text{S}$ (‰)	$\Delta^{36}\text{S}$ (‰)
<i>PPS</i>				
0.1	0.1	0.3	0.009	0.02
0.0	0.0	0.0	0.005	-0.01
-0.1	-0.2	-0.3	-0.014	0.00
<i>Cysteine</i>				
13.7	26.8	52.1	-0.030	0.46
13.7	26.8	51.9	-0.023	0.34
13.4	26.3	51.0	-0.027	0.39
14.4	28.2	54.6	-0.015	0.37

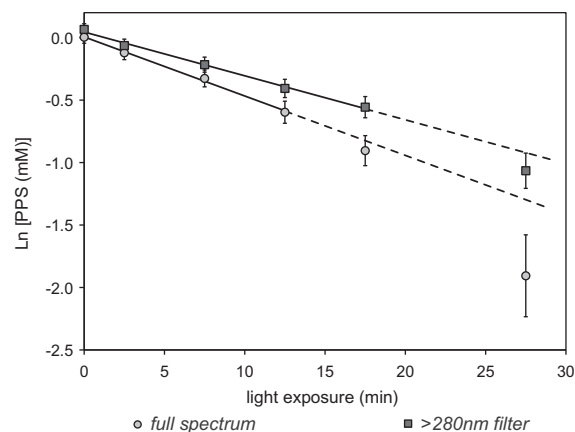


Fig. 3. Plot of the natural logarithm of residual PPS concentration  $[\text{PPS}_r]$  vs. time of exposure during photolysis of PPS for full spectrum (O) and  $>280$  nm filtered light regime (□). The reaction follows first order kinetics until approximately 45% of PPS is degraded (indicated by transition from solid to dashed regression lines). This occurs 12.5/17.5 min into the experiment for full spectrum/filtered light, respectively. The slope of the plotted linear least squares fit signifies the negative first order rate constant of the reaction in this time interval.

The first order rate constant  $k$  over this time interval is calculated to be  $k_{\text{full}} = 0.047 \text{ min}^{-1}$  (half-life: 14.7 min,  $R^2 = 0.997$ ) and  $k_{280} = 0.035 \pm \text{min}^{-1}$  (half-life: 19.8 min,  $R^2 = 0.995$ ) respectively (Fig. 3). After 12.5/17.5 min of photolysis (full spectrum/filtered light), the reaction started to significantly deviate from first order kinetics.

Analysis of the sulfur isotope ratios in the residual PPS after photolysis provided high precision data to assess the mass-independent isotope fractionation during photolysis of PPS (Table 2). Fig. 4 shows the sulfur-MIF created from PPS photolysis at the five measured time points (after 2.5, 7.5, 12.5, 17.5 and 27.5 min of photolysis) for each light regime. The results show that  ${}^{33}\text{S}$  is mass-independently fractionated by  $-2.1\%$  to  $+6.4\%$  while there is no detectable MIF in  ${}^{36}\text{S}$  ( $\Delta^{36}\text{S}$  values range from  $-0.05\%$  to  $+0.09\%$ , which is within the analytical precision of  $\pm 0.19\%$ ). The magnitude of mass-dependent fractionation is smaller than the anomalous isotope effect. The observed  ${}^{34}\text{S}$  values are less than  $2.2\%$  (Table 2), suggesting that there are no major mass-dependent isotope effects during the photolysis of PPS.

For both light spectra (full and filtered), residual PPS is depleted in  ${}^{33}\text{S}$  relative to mass scaling predictions (i.e.  $\Delta^{33}\text{S} < 0\%$ ) for photolysis experiments lasting 15–20 min. For longer times of photolysis on the contrary, residual PPS becomes enriched in  ${}^{33}\text{S}$  relative to mass scaling predictions ( $\Delta^{33}\text{S} > 0\%$ ). The inversion from depletion to enrichment occurs at an earlier time during full spectrum photolysis (after 17 min) with the most depleted residual PPS at 7.5 min. With the 280 nm light filter, the switch occurs after 20 min with the most depleted PPS measured at 12.5 min.

Our results (Table 2) demonstrate that an anomalous  ${}^{33}\text{S}$  abundance (from  $-2.1\%$  to  $+6.4\%$ ) can be produced in

Table 2

Multiple sulfur isotope compositions of residual PPS ( $[\text{PPS}_r]$ ) after photolysis, relative to initial PPS ( $[\text{PPS}_i]$ ).

Photolysis		Isotope fractionation				
Light (min)	$[\text{PPS}_r]$ (mM)	$\delta^{33}\text{S}$ (‰)	$\delta^{34}\text{S}$ (‰)	$\delta^{36}\text{S}$ (‰)	$\Delta^{33}\text{S}$ (‰)	$\Delta^{36}\text{S}$ (‰)
<i>Full spectrum</i>						
0.0	1.00	0.0	0.0	0.0	0.000	0.00
2.5	0.89	-0.6	0.7	1.4	-0.952	0.09
7.5	0.72	-1.9	0.5	1.0	-2.144	-0.02
12.5	0.55	-0.8	1.3	2.5	-1.509	0.05
17.5	0.40	1.0	1.1	2.0	0.491	-0.03
27.5	0.15	7.6	2.1	4.2	6.444	0.07
<i>&gt;280 nm filter</i>						
0.0	1.07	0.0	0.0	0.0	0.000	0.00
2.5	0.94	-0.8	-0.1	-0.3	-0.738	-0.01
7.5	0.81	-1.6	0.3	0.6	-1.734	0.06
12.5	0.67	-1.7	0.4	0.8	-1.859	0.03
17.5	0.57	-0.1	1.3	2.4	-0.752	0.06
27.5	0.34	4.0	1.2	2.2	3.380	-0.05

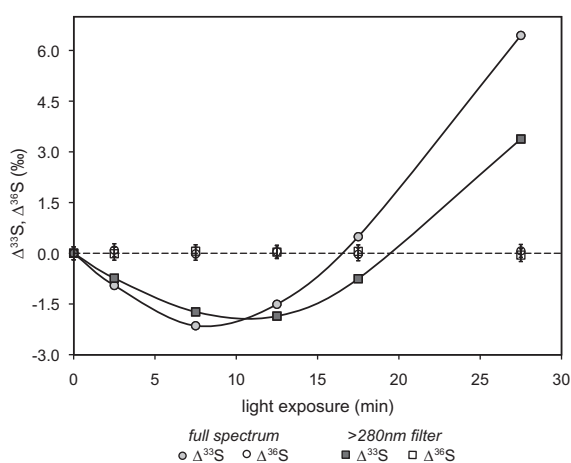


Fig. 4. Plot of  $\Delta^{33}\text{S}$  and  $\Delta^{36}\text{S}$  in residual PPS over the course of photolysis for full spectrum ( $\circ$ ) and  $>280\text{ nm}$  filtered light ( $\square$ ). Uncertainties for these data are smaller than the symbol sizes.

liquid phase chemistry without accompanying  $^{36}\text{S}$  anomaly. This corroborates the presence and importance of a magnetic isotope effect (MIE) as suggested by Step et al. (1992).

## 4. DISCUSSION

### 4.1. PPS photolysis

The apparent adherence to first order kinetics at the beginning of PPS photolysis is in agreement with the expected overall reaction mechanism for photolysis, as is the higher rate constant/faster degradation for the full spectrum. The relatively small decrease in photolytic rate from full to filtered spectrum (26%) suggests that  $\pi \rightarrow \pi^*$  transitions (absorption peak at 254 nm, Fig. 2) do not contribute to the photolysis. Instead, PPS photolysis is mediated by  $n \rightarrow \pi^*$  transitions from light absorption at longer wavelengths, primarily  $>280\text{ nm}$ . This confirms the earlier observation by Step et al. (1992) that short wavelength UV is not

required for this process to occur, allowing associated isotopic effects for similar organic sulfur compounds (with ketone or sulfone functional groups) to occur even in the presence of ozone shielding in a slightly oxic atmosphere ( $\sim 10^{-2}$  PAL  $\text{O}_2$ , Farquhar et al., 2001).

The observed deviations from first order kinetics for extended times of light exposure are possibly due to secondary effects from the accumulation of reaction products once a substantial portion of PPS ( $>45\%$ ) has already been photolyzed. While only hinted at vaguely in the deviation from first-order kinetics, the observed sign reversal in the  $^{33}\text{S}$  anomaly strongly suggests significant changes in reaction dynamics over the course of photolysis as discussed below.

### 4.2. Magnetic isotope effects during PPS photolysis

The clear signal of a negative  $^{33}\text{S}$  anomaly in the residual PPS, with  $\Delta^{33}\text{S}$  values depleted as low as  $-2.1\text{‰}$  was unexpected as previous research observed  $^{33}\text{S}$  enrichment in the residual PPS (Step et al., 1992). Not only the sign of the effect differs from previous results, the magnitude of the anomaly decreases and reverses with time, suggesting temporally changing contributions of at least two separate spin-selective processes. Rescaling the  $\Delta^{33}\text{S}$  values for the different light conditions (full spectrum and  $>280\text{ nm}$ ) by the fraction of total PPS photolyzed at each time point respectively reveals that the results from two experiments with different light spectra (full and filtered) follow the same trajectory, i.e., when the same amount of PPS is photolyzed (regardless of the light spectrum and how long photolysis has to proceed to reach this point), the residual PPS will have the same isotopic composition. This implies that the observed change in  $\Delta^{33}\text{S}$  solely depends on the disappearance of PPS (or more likely, the concomitant appearance of reaction products).

#### 4.2.1. Estimating instantaneous fractionation

The instantaneous fractionation factor between successive time points provides a measure of this isotopic variation

(Table 3) and can be derived from experimental data by applying the conventional formula for closed system isotope effects (e.g., Mariotti et al., 1981):

$${}^{33}\alpha - 1 = \frac{\ln \frac{{}^{33}R_2}{{}^{33}R_1}}{\ln \frac{[\text{PPS}_2]}{[\text{PPS}_1]}} \quad (5)$$

where [PPS] is the concentration and  ${}^{33}R$  the  ${}^{33}\text{S}/{}^{32}\text{S}$  ratio of PPS at time points  $t_1$  and  $t_2$ , respectively. This  ${}^{33}\alpha$  value includes contributions from mass-independent and mass-dependent isotope effects. Only small mass-dependent fractionation of less than 2.1‰ was observed (Table 2) and the fractionation factor due to the anomalous, presumably magnetic, isotope effect ( ${}^{33}\alpha_{\text{MIE}}$ ) can be approximated as:

$$\alpha_{\text{MIE}} - 1 \approx \frac{\Delta^{33}S_2 - \Delta^{33}S_1}{\ln([\text{PPS}_2]) - \ln([\text{PPS}_1])} \quad (6)$$

Plotted against the average photolyzed PPS fraction between two time points  $\text{PPS}_{\text{ph}} = 1 - \sqrt{[\text{PPS}_1][\text{PPS}_2]}/\text{PPS}_0$  (i.e., product accumulated), the derived fractionation factor shows the light spectrum independent change in direction of the mass-independent magnetic isotope effect from  ${}^{33}\alpha_{\text{MIE}} > 1$  ( ${}^{33}\text{S}$  depletion in residual PPS) to  ${}^{33}\alpha_{\text{MIE}} < 1$  ( ${}^{33}\text{S}$  enrichment in residual PPS) as the reaction progresses. The photolysis of PPS produced  ${}^{33}\alpha_{\text{MIE}}$  as high as  $1.008 \pm 0.003$  ( $8 \pm 3\%$ ) at the beginning of photolysis, switched sign after the degradation of approximately 0.35 mM PPS (35% of starting pool), and reached fractionation factors as low as  $0.992 \pm 0.002$  ( $-8 \pm 2\%$ ) that seem to level out towards the end of photolysis (Fig. 5). The trajectories from both light spectra closely match within experimental error and highlight the sole dependence of the observed isotope variations on the fraction of PPS photolyzed (or reaction products formed), irrespective of overall photolytic rate or light regimes for excitation.

#### 4.2.2. Reaction pathways and the sign and magnitude of the MIE

The original model of PPS photolysis illustrated in Fig. 1 would always lead to accumulation of  ${}^{33}\text{S}$  (i.e.,  ${}^{33}\alpha_{\text{MIE}} < 1$ ) in the residual PPS. Sign reversal and  ${}^{33}\text{S}$  depletion cannot be explained by this model, and  ${}^{33}\text{S}$  enrichment

Table 3

Instantaneous fractionation factor  ${}^{33}\alpha_{\text{MIE}}$  between successive time points.

Photolysis interval (min)	$[\text{PPS}_{\text{ph}}]$ (mM)	${}^{33}\alpha_{\text{MIE}}$
<i>Full spectrum</i>		
0–2.5	0.06	$1.0076 \pm 0.0031$
2.5–7.5	0.20	$1.0058 \pm 0.0016$
7.5–12.5	0.37	$0.9976 \pm 0.0006$
12.5–17.5	0.53	$0.9935 \pm 0.0020$
17.5–27.5	0.76	$0.9941 \pm 0.0009$
<i>&gt;280 nm filter</i>		
0–2.5	0.07	$1.0057 \pm 0.0030$
2.5–7.5	0.20	$1.0065 \pm 0.0023$
7.5–12.5	0.34	$1.0007 \pm 0.0002$
12.5–17.5	0.45	$0.9926 \pm 0.0038$
17.5–27.5	0.62	$0.9919 \pm 0.0015$

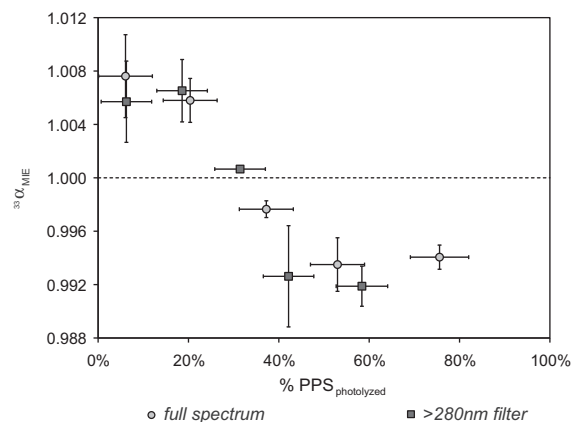


Fig. 5. Fractionation factor derived from experimental data for full spectrum photolysis (○) and >280 nm filtered light regime (■), plotted against fraction of photolyzed PPS. All errors derived by error propagation.

was only observed during the later stage of our PPS photolysis experiments. The change of sign can also not be explained by closed system (Rayleigh) effects but rather suggests temporally changing contributions of at least two separate spin-selective pathways. Here we discuss two reaction mechanisms that could explain our observations.

**4.2.2.1. Sign reversal by changing spin multiplicity.** Apparent inverse magnetic isotope effects have been observed for magnetic mercury isotopes ( ${}^{199}\text{Hg}$  and  ${}^{201}\text{Hg}$ ) during photolysis of an organo-Hg compound (bis(*p*-trifluoromethylbenzyl) mercury; Buchachenko et al., 2008) and during photochemical reduction of  $\text{Hg}^{2+}$  by some simple organosulfur compounds (e.g., cysteine, methionine, thiourea, glutathione; Zheng and Hintelmann, 2010). The inversion is suggested to occur due to the presence of a photolytic decomposition pathway that proceeds via a singlet radical pair ( ${}^1\text{RP}$ ). The spin multiplicity of the starting RP (triplet vs. singlet) determines whether decomposition leads to enrichment (triplet) or depletion (singlet) of magnetic isotopes in the starting material.

The reaction scheme presented earlier (Fig. 1) illustrates PPS decomposition via triplet radical pair ( ${}^3\text{RP}$ ) leading to  ${}^{33}\text{S}$  enrichment (Scheme 1). Fig. 6 (Scheme 2) extends Scheme 1 to include PPS decomposition via singlet radical pair ( ${}^1\text{RP}$ ) leading to  ${}^{33}\text{S}$  depletion in residual PPS. In Scheme 2, ground state PPS ( $S_0$ ) also absorbs a photon to produce the electronically excited singlet state ( $S_1$ ), but then generates a singlet radical pair ( ${}^1\text{RP}$ ). This  ${}^1\text{RP}$  either recombines to form PPS ( $k_{\text{RC}}$ ) or undergoes singlet-triplet inter system crossing ( $k_{\text{S-T}}$ ) to form the triplet RP ( ${}^3\text{RP}$ ), which diffuses and reacts to form reaction products ( $k_{\text{D}}$ ). Similar to Scheme 1, hyperfine interaction (HFI) between the magnetic  ${}^{33}\text{S}$  nuclei and electron spin moments accelerates the spin conversion of the RP. Instead of  ${}^{33}\text{S}$  enrichment, however, Scheme 2 leads to depletion of  ${}^{33}\text{S}$  in residual PPS (Fig. 6). A temporally changing combination of both Scheme 1 and 2 could explain our observations: if photolysis proceeds predominantly via the singlet RP (following Scheme 2) at the beginning of our experiment, the

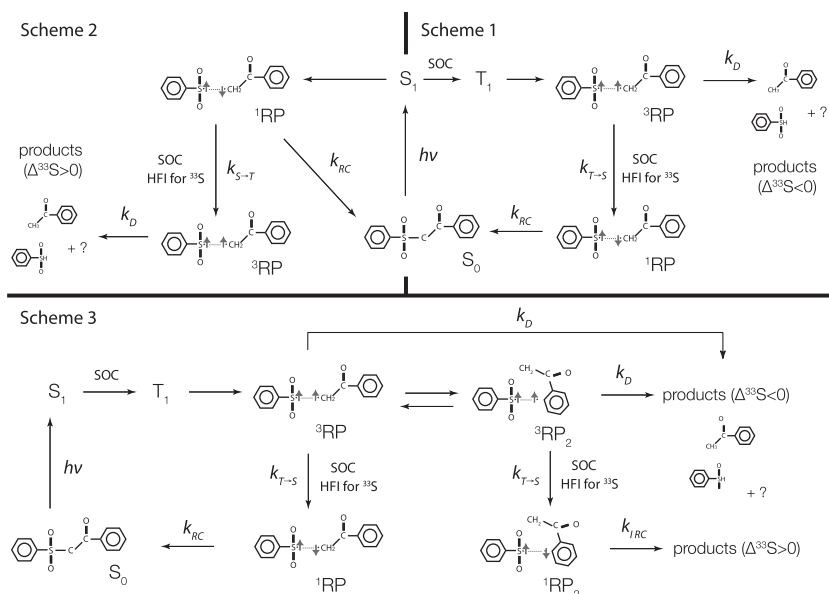


Fig. 6. Potential reaction pathways of PPS photolysis. Intersystem crossing (ISC) by hyperfine interaction (HFI) during spin conversion of triplet ( $^3\text{RP}$ ) to singlet radical pair ( $^1\text{RP}$ ) and vice-versa is accelerated by the magnetic isotope  $^{33}\text{S}$  and produces a magnetic isotope effect. Mechanisms, electronic states and pathways mentioned in the text are indicated: spin-orbit coupling (SOC); ground state ( $\text{S}_0$ ), singlet ( $\text{S}_1$ ) and triplet ( $\text{T}_1$ ) PPS; misaligned radical pair ( $\text{RP}_2$ ); RP diffusion ( $k_{\text{D}}$ ); triplet-singlet ( $k_{\text{T}\rightarrow\text{S}}$ ) and singlet-triplet ( $k_{\text{S}\rightarrow\text{T}}$ ) ISC; correct RP recombination to PPS ( $k_{\text{RC}}$ ) and incorrect recombination ( $k_{\text{IRC}}$ ). Indicated  $\Delta^{33}\text{S}$  of reaction products illustrates nominal  $^{33}\text{S}$  enrichment/depletion of each pathway but in Scheme 3 depends on the relative contributions of the pathways.

remaining PPS would become depleted in  $^{33}\text{S}$ . Once reaction products accumulate, the excited singlet state of PPS ( $\text{S}_1$ ) is quenched to triplet PPS ( $\text{T}_1$ ), generating triplet RP (following Scheme 1). If the spin evolution of the RP changes in this way from predominantly singlet  $\rightarrow$  triplet (Scheme 2) to predominantly triplet  $\rightarrow$  singlet (Scheme 1), the sign of the isotope effect could change as observed (Fig. 4). Lastly, the magnitude of the observed  $^{33}\text{S}$  anomaly ( $-2.1\%$  to  $6.4\%$ ) is relatively small for a magnetic isotope effect (Step et al., 1992), which could be explained by the co-occurrence of the two pathways and partial compensation of their respective effect on  $^{33}\text{S}$  depletion/enrichment.

**4.2.2.2. Sign reversal by competing triplet radical pairs.** The above described reaction mechanism requires the production of a long lived singlet radical pair ( $\text{S}_1$ ) during PPS photolysis (Scheme 2) since HFI is usually a very slow process (nano to  $\mu\text{s}$ ; Turro and Kraeutler, 1980). However, previous studies have suggested that the excited state of PPS has triplet spin multiplicity ( $\text{T}_1$ ) instead, following rapid singlet to triplet transition from  $\text{S}_1$  (Tsunooka et al., 1983; Hayashi et al., 1987; Step et al., 1992). Additionally, Step et al. (1992) suggest the presence of two separate triplet radical pairs  $^3\text{RP}$  and  $^3\text{RP}_2$ . If this is indeed the case and no long lived  $\text{S}_1$ , but two triplet radical pairs exist instead, the observed sign flip for the measured  $^{33}\alpha_{\text{MIE}}$  could be explained by considering an additional decomposition pathway available to the second triplet radical pair (Fig. 6, Scheme 3): after the formation of the initial triplet radical pair ( $^3\text{RP}$ ) by the original pathway (Scheme 1), the radical pair can

reorient to form a similar second triplet radical pair ( $^3\text{RP}_2$ ), which can also undergo triplet-singlet ISC through electron–nuclear hyperfine interactions (favoring  $^{33}\text{S}$ ) in competition with radical pair diffusion ( $k_{\text{D}}$ ), but will no longer recombine correctly to restore the original PPS, instead forming an unstable intermediate destined to break apart ( $k_{\text{IRC}}$ ) and contribute to the pool of reaction products. As pointed out by Step et al. (1992), the two different triplet radical pairs appear to differ mostly in the details of their diffusional history and possibly stereostructure in the micellar cage provided by the SDS solution. Consequently, it is conceivable that their reaction rates are influenced differently by the accumulation of reaction products inside the micelle, thus shifting the relative contributions from the two escape pathways for the triplet radical pair in a product-dependent pattern over the course of photolysis in a way that reflects in the change in fractionation factor observed in this study. The relatively small magnitude of the observed  $^{33}\text{S}$  anomaly in this case would indicate that not only the balance between the separate HFI mediated spin-selective pathways, but also competition with SOC diminish the observed MIE (see Fig. 6) since SOC is a coupling of electron spin to electron orbital motion that is independent of nuclear spin and does not produce an isotopic effect.

Although a more detailed mechanistic understanding of PPS photolysis and testing of the proposed reaction pathways is beyond the scope of this study, our results demonstrate that magnetic isotope effects in  $^{33}\text{S}$  can produce MIE in both directions and are likely modulated by competing reaction pathways.

#### 4.3. Required conditions for sulfur MIE

One of the postulates of the magnetic isotope effect is that MIE is produced by hyperfine interactions (HFI) of radical pairs. Although photochemistry is a good initiator of radical pair chemistry (e.g., studies by Buchachenko (1995), Bergquist and Blum (2007), Zheng and Hintelmann (2010), Sherman et al. (2010)), MIE is not exclusive to photochemistry (Turro and Chow, 1980; Buchachenko et al., 1984; Buchachenko et al., 2007). Turro and Chow (1980) demonstrated the production of oxygen isotope MIE during the thermolysis of diphenylanthracene endoperoxide at 90 °C, suggesting the thermolysis proceeds through triplet diradical formation. Oduro et al. (2011) recently reported evidence for sulfur MIE during thermochemical reduction of sulfate with simple amino acids at 300 °C (following an earlier report by Watanabe et al. (2009)) and suggested the formation of thio-disulfide radical pairs as reaction intermediates. Sulfur radicals are also known to occur in biological systems and are increasingly recognized for their role in radical based catalysis and redox sensing (Glass, 1999; Sofia et al., 2001; Bauer et al., 2008). Buchachenko et al. (2004), for example, report thermal production of sulfur radicals from cysteine residues at 30 °C.

In addition to the presence of radical pairs, a second critical condition for the production of MIE is a sufficiently long lifetime of the radical pair such that spin-forbidden transitions become accessible by HFI (Turro and Kraeutler, 1980) (gas phase reactions tend not to satisfy this condition). Slower diffusion rates in liquid and solid-phase are favorable towards the occurrence of HFI as demonstrated, for example, by the common occurrence of Hg-MIE in aqueous environments (Bergquist and Blum, 2007; Zheng and Hintelmann, 2010), and MIE in polymer films or porous glass (Turro and Kraeutler, 1980). Accordingly, further restriction of the chemical or diffusional environment can also favor the effect. This can be observed for reactions in a micellar cage (this study, Turro, 1983; Hayashi et al., 1987; Step et al., 1992) and, conceivably, the diffusional restricted environment of cellular lipid membranes.

MIE is unlikely to occur in gas phase reactions because the fast diffusive decay of radical pairs would not allow slow HFI to take place (Bhattacharya et al., 2000). On the contrary, other mechanisms for MIF, such as isotope self-shielding (Lyons and Young, 2005; Lyons, 2009) and energy level matching during curve crossing (Zmolek et al., 1999; Bhattacharya et al., 2000; Chakraborty et al., 2008) are unlikely to produce MIF in liquid phase chemistry. For the self-shielding or curve crossing mechanism to be isotope selective, two crossing states have to show well defined vibrational fine structure with features sharper than the energy level shift due to isotopic substitution. Several gas phase sulfur-bearing molecules (e.g., SO<sub>2</sub> and CS<sub>2</sub>) show such vibrational fine structure in the UV spectrum (Danielache et al., 2008b; Lyons, 2008). In liquid phase, however, the energy levels become broadened due to solvent interactions (smooth absorption spectrum of PPS in micellar SDS solution is visible in Fig. 2). This broadening is strongest for polar solvents as a consequence of hydrogen bonding, but also occurs for non-polar solvents due to

London dispersion forces. The lack of vibrational fine structure in liquid phase makes self-shielding and curve crossing effects highly unlikely to occur.

#### 4.4. MIE and the Archean multiple sulfur isotope record

In Fig. 7, the observed MIE is compared to the  $\Delta^{33}\text{S}$  and  $\Delta^{36}\text{S}$  values measured from Archean rocks. While the magnitude of the MIE observed in this study is comparable to that of  $\Delta^{33}\text{S}$  values measured in Archean rocks, the striking discrepancy in  $\Delta^{36}\text{S}$  illustrates the divide between MIE and Archean multiple sulfur isotope trends. It is evident that an MIE, such as the one observed from the experiments in this study, cannot constitute the principal source of mass-independent signals observed for Archean samples.

### 5. CONCLUSION

A decade after first evidence for the preservation of a strong mass-independent sulfur signal in the Archean rock record was published, the precise origin of the Archean mass-independent sulfur signal remains elusive. This study was aimed at investigating the potential contribution of the poorly explored mass-independent effects from liquid phase sulfur chemistry and focused on sulfur isotope fractionation during liquid phase, light regime dependent photolytic breakdown of PPS as a model system for initial investigation. The results of this study provide evidence that liquid phase processes such as the photolysis of PPS can produce significant mass-independent fractionation ( $\Delta^{33}\text{S}$  ranging from  $-2.1\text{‰}$  to  $6.4\text{‰}$ ). The purely mass-dependent fractionation among the non-magnetic sulfur isotopes (<sup>32</sup>S, <sup>34</sup>S, <sup>36</sup>S) confirms the effect to be magnetic in nature. The range in the observed <sup>33</sup>S anomaly from depletion to enrichment suggests at least two separate spin-selective processes to co-occur during the photolysis.

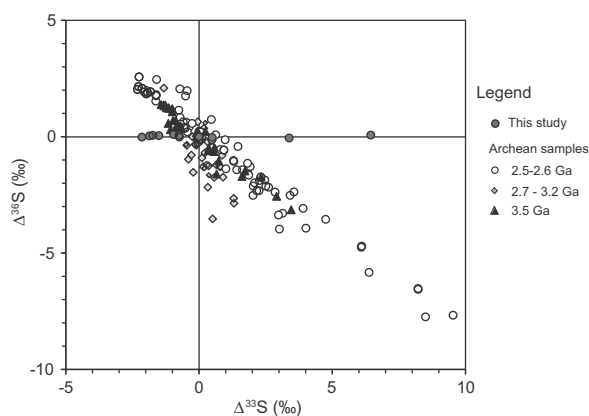


Fig. 7.  $\Delta^{36}\text{S}$  vs.  $\Delta^{33}\text{S}$  for the experimental product (this study) compared to those measured for Archean rocks. Data from Archean rocks are divided by age of samples, showing similar overall trend for the late and early Archean (3.45 Ga) but potentially different systematics during middle Archean (2.7–3.2 Ga). Data sources are Kaufman et al. (2007), Farquhar et al. (2007), Ono et al. (2006a, 2009), Ueno et al. (2008).

The sulfur MIE observed in this study does not require high energy UV light (<280 nm). Similar reactions that produce S-MIF could exist in natural environments even under a weak ozone shield. Such reactions are likely exclusive to liquid and solid phase chemistry where HFI can compete with the diffusional loss of radical pairs. Magnetic isotope effects cannot constitute the principal source of mass-independent fractionation in the Archean due to the lack of a concomitant  $\Delta^{36}\text{S}$  anomaly.

#### ACKNOWLEDGEMENTS

We thank William Olszewski, Nicole Keller, and Evelyn Corder for technical assistance. Alexander Petroff and Chris Kempes for helpful discussions. Mark Thiemens, Huiming Bao, James Farquhar, and anonymous reviewers for their constructive comments that improved the manuscript. This work was supported by the NASA exobiology program (Grant #NNX074U12G and NNX10AR85G).

#### REFERENCES

- Angert A., Rachmilevitch S., Barkan E. and Luz B. (2003) Effects of photorespiration, the cytochrome pathway, and the alternative pathway on the triple isotopic composition of atmospheric  $\text{O}_2$ . *Global Biogeochem. Cycles* **17**(1), 1030.
- Arikawa Y. and Sasaki A. (1987) Extraction and isotope measurement of sulfur in biological samples. *Anal. Sci.* **3**, 1–4.
- Bauer G., Chatgililoglu C., Gebicki J. L., Gebicka L., Gescheidt G., Golding B. T., Goldstein S., Kaizer J., Merenyi G., Speier G. and Wardman P. (2008) Biologically relevant small radicals. *Chimia* **62**(9), 704–712.
- Bekker A., Holland H., Wang P., Rumble D., Stein H., Hannah J., Coetzee L. and Beukes N. (2004) Dating the rise of atmospheric oxygen. *Nature* **427**(6970), 117–120.
- Bergquist B. A. and Blum J. D. (2007) Mass-dependent and -independent fractionation of Hg isotopes by photoreduction in aquatic systems. *Science* **318**(5849), 417–420.
- Bhattacharya S., Savarino J. and Thiemens M. (2000) A new class of oxygen isotopic fractionation in photodissociation of carbon dioxide: Potential implications for atmospheres of Mars and Earth. *Geophys. Res. Lett.* **27**(10), 1459–1462.
- Bigeleisen J. (1996) Nuclear size and shape effects in chemical reactions. Isotope chemistry of the heavy elements. *J. Am. Chem. Soc.* **118**(15), 3676–3680.
- Bigeleisen J. and Mayer M. G. (1947) Calculation of equilibrium constants for isotopic exchange reactions. *J. Chem. Phys.* **15**(5), 261–267.
- Buchachenko A., Fedorov A., Yasina L. and Galimov E. (1984) The magnetic isotope effect and oxygen isotope selection in chain processes of polymer oxidation. *Chem. Phys. Lett.* **103**(5), 405–407.
- Buchachenko A. L. (1995) The nuclear-spin selectivity of chemical reactions. *Russ. Chem. Rev.* **64**(9), 863–871.
- Buchachenko A. L. (2001) Magnetic isotope effect: nuclear spin control of chemical reactions. *J. Phys. Chem. A* **105**(44), 9995–10011.
- Buchachenko A. L., Ivanov V. L., Roznyatovskii V. A., Vorob'ev A. K. and Ustynuk Y. A. (2008) Inversion of the sign of the magnetic isotope effect of mercury in photolysis of substituted dibenzylmercury. *Dokl. Phys. Chem.* **420**, 85–87.
- Buchachenko A. L., Kouznetsov D. A. and Shishkov A. V. (2004) Spin biochemistry: magnetic isotope effect in the reaction of creatine kinase with  $\text{CH}_3\text{HgCl}$ . *J. Phys. Chem. A* **108**(5), 707–710.
- Buchachenko A. L., Lukzen N. N. and Pedersen J. B. (2007) On the magnetic field and isotope effects in enzymatic phosphorylation. *Chem. Phys. Lett.* **434**(1–3), 139–143.
- Cartigny P., Farquhar J., Assayag N. and Bourrand J. (2008) Experimental evidence for mass independent fractionation of sulfur isotopes without any UV-photolysis or glow discharge. *Eos Trans. AGU* **89**(53) Fall Meet. Suppl. (abstract V52B-03).
- Chakraborty S., Ahmed M., Jackson T. and Thiemens M. (2008) Experimental test of self-shielding in vacuum ultraviolet photodissociation of  $\text{CO}$ . *Science* **321**(5894), 1328.
- Danielache S., Johnson M., Nanbu S., Grage M., Mclinden C. and Yoshida N. (2008a) Ab initio study of sulfur isotope fractionation in the reaction of OCS with OH. *Chem. Phys. Lett.* **450**(4–6), 214–220.
- Danielache S. O., Eskebjerg C., Johnson M. S., Ueno Y. and Yoshida N. (2008b) High-precision spectroscopy of 32s, 33s, and 34s sulfur dioxide: ultraviolet absorption cross sections and isotope effects. *J. Geophys. Res.* **113**(D17314), 14.
- Farquhar J., Bao H. and Thiemens M. (2000a) Atmospheric influence of Earth's earliest sulfur cycle. *Science* **289**(5480), 756–758.
- Farquhar J., Peters M., Johnston D. T., Strauss H., Masterson A., Wiechert U. and Kaufman A. J. (2007) Isotopic evidence for Mesoarchean anoxia and changing atmospheric sulphur chemistry. *Nature* **449**(7163), 706–U5.
- Farquhar J., Savarino J., Airieau S. and Thiemens M. (2001) Observation of wavelength-sensitive mass-independent sulfur isotope effects during  $\text{SO}_2$  photolysis: implications for the early atmosphere. *J. Geophys. Res. Planets* **106**(E12), 32829–32839.
- Farquhar J., Savarino J., Jackson T. and Thiemens M. (2000b) Evidence of atmospheric sulphur in the martian regolith from sulphur isotopes in meteorites. *Nature* **404**(6773), 50–52.
- Farquhar J. and Wing B. (2003) Multiple sulfur isotopes and the evolution of the atmosphere. *Earth Planet. Sci. Lett.* **213**(1–2), 1–13.
- Forrest J. and Newman L. (1977) Silver-110 microgram sulfate analysis for the short time resolution of ambient levels of sulfur aerosol. *Anal. Chem.* **49**(11), 1579–1584.
- Francisco J., Lyons J. and Williams I. (2005) High-level ab initio studies of the structure, vibrational spectra, and energetics of S-3. *J. Chem. Phys.* **123**(5), 054302.
- Gao Y. and Marcus R. (2002) On the theory of the strange and unconventional isotopic effects in ozone formation. *J. Chem. Phys.* **116**(1), 137–154.
- Glass R. (1999) Sulfur radical cations. *Top. Curr. Chem.* **205**, 1–87.
- Hayashi H., Sakaguchi Y., Tsunooka M., Yanagi H. and Tanaka M. (1987) Laser flash photolysis study of magnetic field effects on the photodecomposition of phenacyl phenyl sulfone in micellar solution. *Chem. Phys. Lett.* **136**(5), 436–440.
- Kasting J. (2001) Earth history – the rise of atmospheric oxygen. *Science* **293**(5531), 819–820.
- Kaufman A. J., Johnston D. T., Farquhar J., Masterson A. L., Lyons T. W., Bates S., Anbar A. D., Arnold G. L., Garvin J. and Buick R. (2007) Late Archean biospheric oxygenation and atmospheric evolution. *Science* **317**(5846), 1900–1903.
- Lasaga A. C., Otake T., Watanabe Y. and Ohmoto H. (2008) Anomalous fractionation of sulfur isotopes during heterogeneous reactions. *Earth Planet. Sci. Lett.* **268**(1–2), 225–238.
- Lin Y., Sim M. S. and Ono S. (2011) Multiple-sulfur isotope effects during photolysis of carbonyl sulfide. *Atmos. Chem. Phys. Dis.* **11**(5), 14233–14258.
- Lyons A. R. (2008) Photolysis of long-lived predissociative molecules as a source of mass-independent isotope fractionation: the example of  $\text{SO}_2$ . *Adv. Quantum Chem.* **55**, 57–74.

- Lyons J. and Young E. (2005) CO self-shielding as the origin of oxygen isotope anomalies in the early solar nebula. *Nature* **435**(7040), 317–320.
- Lyons J. R. (2009) Atmospherically-derived mass-independent sulfur isotope signatures, and incorporation into sediments. *Chem. Geol.* **267**(3–4), 164–174.
- Mariotti A., Germon J., Hubert P., Kaiser P., Letolle R., Tardieux A. and Tardieux P. (1981) Experimental determination of nitrogen kinetic isotope fractionation: some principles; illustration for the denitrification and nitrification processes. *Plant Soil* **62**, 413–430.
- Masterson A. L., Farquhar J. and Wing B. A. (2011) Sulfur mass-independent fractionation patterns in the broadband UV photolysis of sulfur dioxide: pressure and third body effects. *Earth Planet. Sci. Lett.* **306**(3–4), 253–260.
- Mojzsis S., Coath C., Greenwood J., McKeegan K. and Harrison T. (2003) Mass-independent isotope effects in Archean (2.5–3.8 Ga) sedimentary sulfides determined by ion microprobe analysis. *Geochim. Cosmochim. Acta* **67**(9), 1635–1658.
- Oduro H., Harms B., Sintim H., Kaufman A., Cody G. and Farquhar J. (2011) Evidence of magnetic isotope effects during thermochemical sulfate reduction. *Proc. Natl. Acad. Sci.* **108**(43), 17635–17638.
- Ono S., Beukes N. J., Rumble D. and Fogel M. L. (2006a) Early evolution of atmospheric oxygen from multiple-sulfur and carbon isotope records of the 2.9 Ga Mozaan Group of the Pongola Supergroup, Southern Africa. *S. Afr. J. Geol.* **109**(1–2), 97–108.
- Ono S., Eigenbrode J., Pavlov A., Kharecha P., Rumble D., Kasting J. and Freeman K. (2003) New insights into Archean sulfur cycle from mass-independent sulfur isotope records from the Hamersley Basin, Australia. *Earth Planet. Sci. Lett.* **213**(1–2), 15–30.
- Ono S., Kaufman A. J., Farquhar J., Sumner D. Y. and Beukes N. J. (2009) Lithofacies control on multiple-sulfur isotope records and Neoproterozoic sulfur cycles. *Precambrian Res.* **169**(1–4), 58–67.
- Ono S., Wing B., Johnston D., Farquhar J. and Rumble D. (2006b) Mass-dependent fractionation of quadruple stable sulfur isotope system as a new tracer of sulfur biogeochemical cycles. *Geochim. Cosmochim. Acta* **70**(9), 2238–2252.
- Pavlov A. and Kasting J. (2002) Mass-independent fractionation of sulfur isotopes in Archean sediments: strong evidence for an anoxic Archean atmosphere. *Astrobiology* **2**(1), 27–41.
- Pavlov A., Mills M. and Toon O. (2005) Mystery of the volcanic mass-independent sulfur isotope fractionation signature in the Antarctic ice core. *Geophys. Res. Lett.* **32**(12), L12816.
- Quickenden T. I. and Irvin J. A. (1980) The ultraviolet absorption spectrum of liquid water. *J. Chem. Phys.* **72**(8), 4416–4428.
- Schauble E. A. (2007) Role of nuclear volume in driving equilibrium stable isotope fractionation of mercury, thallium, and other very heavy elements. *Geochim. Cosmochim. Acta* **71**(9), 2170–2189.
- Sherman L. S., Blum J. D., Johnson K. P., Keeler G. J., Barres J. A. and Douglas T. A. (2010) Mass-independent fractionation of mercury isotopes in Arctic snow driven by sunlight. *Nat. Geosci.* **3**(3), 173–177.
- Sofia H., Chen G., Hetzler B., Reyes-Spindola J. and Miller N. (2001) Radical SAM, a novel protein superfamily linking unresolved steps in familiar biosynthetic pathways with radical mechanisms: functional characterization using new analysis and information visualization methods. *Nucleic Acids Res.* **29**(5), 1097–1106.
- Step E. N., Buchachenko A. L. and Turro N. J. (1992) Magnetic effects in the photolysis of micellar solutions of phenacylsulfone. *Chem. Phys.* **162**(1), 189–204.
- Thiemens M. and Heidenreich J. (1983) The mass-independent fractionation of oxygen: a novel isotope effect and its possible cosmochemical implications. *Science* **219**(4588), 1073–1075.
- Thiemens M. H. (2006) History and applications of mass-independent isotope effects. *Ann. Rev. Earth Planet. Sci.* **34**(1), 217–262.
- Thode H. G., Monster J. and Dunford H. B. (1961) Sulphur isotope geochemistry. *Geochim. Cosmochim. Acta* **25**(3), 159–174.
- Tsunooka M., Tanaka S. and Tanaka M. (1983) Photocrosslinking of poly(2,3-epoxypropyl methacrylate) films with organic sulfur-compounds. *Makromol. Chem. Rapid* **4**(8), 539–541.
- Turro N. J. (1983) Influence of nuclear spin on chemical reactions: magnetic isotope and magnetic field effects (a review). *PNAS* **80**(2), 609–621.
- Turro N. J. and Chow M.-F. (1980) Magnetic isotope effect on the thermolysis of 9,10-diphenylanthracene endoperoxide as a means of separation of oxygen-17 from oxygen-16 and oxygen-18. *J. Am. Chem. Soc.* **102**(3), 1190–1192.
- Turro N. J. and Kraeutler B. (1980) Magnetic field and magnetic isotope effects in organic photochemical reactions. A novel probe of reaction mechanisms and a method for enrichment of magnetic isotopes. *Acc. Chem. Res.* **13**(10), 369–377.
- Ueno Y., Ono S., Rumble D. and Maruyama S. (2008) Quadruple sulfur isotope analysis of ca. 3.5 Ga Dresser Formation: new evidence for microbial sulfate reduction in the early Archean. *Geochim. Cosmochim. Acta* **72**(23), 5675–5691.
- Urey H. (1947) The thermodynamic properties of isotopic substances. *J. Chem. Soc.*, 562–581.
- Watanabe Y., Farquhar J. and Ohmoto H. (2009) Anomalous fractionations of sulfur isotopes during thermochemical sulfate reduction. *Science* **324**(5925), 370–373.
- Young E., Galy A. and Nagahara H. (2002) Kinetic and equilibrium mass-dependent isotope fractionation laws in nature and their geochemical and cosmochemical significance. *Geochim. Cosmochim. Acta* **66**(6), 1095–1104.
- Zheng W. and Hintelmann H. (2010) Isotope fractionation of mercury during its photochemical reduction by low-molecular-weight organic compounds. *J. Phys. Chem. A* **114**(12), 4246–4253.
- Zmolek P., Xu X., Jackson T., Thiemens M. and Trogler W. (1999) Large mass independent sulfur isotope fractionations during the photopolymerization of (CS<sub>2</sub>)-C-12 and (CS<sub>2</sub>)-C-13. *J. Phys. Chem. A* **103**(15), 2477–2480.

Associate editor: James Farquhar